HHS Public Access

Author manuscript

Nature. Author manuscript; available in PMC 2014 October 17.

Published in final edited form as:

Nature. 2014 April 17; 508(7496): 387–391. doi:10.1038/nature13238.

Rapid and tunable post-translational coupling of genetic circuits

Arthur Prindle[1,★], **Jangir Selimkhanov**[1,★], **Howard Li**[1], **Ivan Razinkov**[1], **Lev S. Tsimring**[2], and **Jeff Hasty**[1,2,3,4]

[1]Department of Bioengineering, University of California, San Diego, La Jolla, California, USA

[2]BioCircuits Institute, University of California, San Diego, La Jolla, California, USA

[3]Molecular Biology Section, Division of Biological Science, University of California, San Diego, La Jolla, CA 92093, USA

Abstract

One promise of synthetic biology is the creation of genetic circuitry that enables the execution of logical programming in living cells. Such “wet programming” is positioned to transform a wide and diverse swath of biotechnology ranging from therapeutics and diagnostics to water treatment strategies. While progress in the development of a library of genetic modules continues apace[1–4], a major challenge for their integration into larger circuits is the generation of sufficiently fast and precise communication between modules[5,6]. An attractive approach is to integrate engineered circuits with host processes that facilitate robust cellular signaling[7]. In this context, recent studies have demonstrated that bacterial protein degradation can trigger a precise response to stress by overloading a limited supply of intracellular proteases[8–10]. Here, we use protease competition to engineer rapid and tunable coupling of genetic circuits across multiple spatial and temporal scales. We characterize coupling delay times that are more than an order of magnitude faster than standard transcription-factor based coupling methods (less than one minute compared with ~20–40 minutes) and demonstrate tunability through manipulation of the linker between the protein and its degradation tag. We use this mechanism as a platform to couple genetic clocks at the intracellular and colony level, then synchronize the multi-colony dynamics to reduce variability in both clocks. We show how the coupled clock network can be used to encode independent environmental inputs into a single time series output, thus enabling the possibility of frequency multiplexing in a genetic circuit context. Our results establish a general framework for the rapid and tunable coupling of genetic circuits through the use of native queueing processes such as protein degradation.

[4]Corresponding Author. Molecular Biology Section, Division of Biological Science, University of California, San Diego, Mailcode 0368, La Jolla, CA 92093-0368, USA. Telephone: 858 822 3442. hasty@ucsd.edu.

★These authors contributed equally to this work.

Extended Data Information

Extended Data information, including methods, supplementary figures and tables, is linked to the online version of the paper at www.nature.com/nature.

Author Contributions

All authors contributed extensively to the work presented in this paper. A.P. and J.S. are equally contributing first authors.

The authors declare no competing financial interests.

In order to engineer rapid coupling between synthetic genetic modules, we developed a post-translational coupling platform that operates via shared degradation by the ClpXP protease (Fig. 1a). In this scheme, all LAA-tagged components[11] are dynamically linked via competition for a limited number of proteases[10, 12], such that tagged modules remain tightly aligned (1±1 min, GFP-CFP curve pairs in Fig. 1a) despite significant induction delay (31±5 min, inducer-GFP offset in Fig. 1a). This coupling method produces delays that are more than an order of magnitude faster than standard transcription-factor based coupling methods (~20–40 min)[13, 14]. To illustrate directly the response time that can be achieved by coordinating module output via modulating ClpXP activity, we show that low levels (90 μM) of externally provided H_2O_2 "inducer" rapidly (< 2 min, our experimental timestep) and reversibly modulates the concentration of constitutively expressed GFP in a ClpXP-dependent manner (Fig. 1b). Here, H_2O_2 reduces the native substrate load on ClpXP by obstructing RssB, the adapter protein that targets the alternative sigma factor σ^S for degradation by ClpXP[8, 9, 15]. Since σ^S is continuously produced and degraded by ClpXP, inactivating its rate-limiting adapter protein results in an instantaneous increase in the effective ClpXP degradation rate for LAA-tagged proteins[16].

We systematically explored the coupling mechanism by driving a constitutive module with a quorum-sensing (Fig. 1c). As the pacemaker, the quorum clock generates density-dependent synchronous oscillations at the colony level via acyl-homoserine lactone (AHL), a small molecule capable of synchronizing cellular behavior across distances up to 100 μm[17]. Using microfluidic devices[18] we observed the colony-level expression of the constitutive module, finding oscillating expression synchronized to the quorum clock (Fig. 1c, top right). We then constructed a library of degradation tags by adding a series of variable-length spacer regions between the downstream protein and its degradation tag. Spacer regions contained between one and five copies of the amino acid sequence "TS" and their effects on offset time compared to that of a previously published alternate degradation tag (Extended Data Fig. 1b–f). While all spacer sequences produced synchronous activation dynamics, the degradation dynamics of the downstream module were offset depending on the length of the linker sequence, where longer linkers produced greater GFP-CFP offset time (Fig. 1C, bottom). Thus, our ClpXP coupling platform rapidly links genetic modules via shared degradation, where the strength and timing of coupling can be tuned by changing the degradation kinetics of individual modules.

In order to engineer coupling between genetic modules capable of generating their own dynamics, we designed a circuit containing the quorum clock and a variant of a previously described intracellular clock (Fig. 2a)[19]. This $P_{lac/ara-1}$ intracellular clock variant retains the fast dynamics and simple genetic architecture of the published $P_{LlacO-1}$ negative feedback oscillator, yet its period is tunable by both isopropyl β-D-1-thiogalactopyranoside (IPTG) and arabinose in the presence of chromosomal araC. We first used small microfluidic devices (100 cells) and observed fast and asynchronous intracellular clock oscillations without quorum clock contribution, since the quorum clock requires a critical colony size to function (Supplementary Video 1 and Extended Data. Microscopy and Microfluidics). In larger devices (5,000 cells), we observed a transition from asynchronous oscillations to identical intracellular/quorum clock oscillations as the population grew larger (Fig. 2b and

Supplementary Video 2). In the case of the larger population, the substrate load on ClpXP during the quorum clock pulse is sufficient to shift the intracellular clock out of its oscillatory regime, enabling complete linkage between the two clocks despite their vastly different spatial and temporal scales. Thus, despite lacking a mode of cell-cell communication itself, the intracellular clock is effectively synchronized at the colony level via ClpXP-mediated coupling with the quorum clock.

We found that changing the intracellular clock period of individual cells indirectly tuned the quorum clock period, where IPTG values associated with longer intracellular clock periods inversely produced shorter quorum clock periods (Fig. 2c). We developed a computational model of the oscillator network involving a form of load-mediated pulse frequency modulation to explain this effect (Fig. 2d–f). Between coupled pulses, the intracellular clock accelerates the quorum pulse onset via load-mediated decreases in the degradation rate of LuxI, where larger intracellular clock load produces higher levels of the AHL-synthase (Fig. 2e, left and Extended Data Fig. 2a–e). During the coupled pulse, contributions of the intracellular clock leave the duration of the pulse itself unchanged (Fig. 2e, left: model and right: experimental). Linking the intracellular and quorum clocks via degradation also yielded an expansion in the oscillatory regime for the coupled system with respect to flow rate compared to the quorum clock alone (Fig. 2f). In this way, the intracellular clock continually excites the quorum clock to fire, enabling more robust function at higher external flow rates (Extended Data Fig. 3a–c).

With a platform for rapidly coupling genetic clocks at multiple scales, we sought to engineer a system capable of frequency encoding information from both clocks into the multispectral time series of a single reporter (Fig. 3a). Here, the measured output of the intracellular clock reporter contains contributions from its own fast intracellular clock dynamics between slow quorum clock bursts (Supplementary Video 3). Since the range of natural periods for the faster $P_{lac/ara-1}$ intracellular clock is fully separated from the slower quorum clock[17, 19, 20], both IPTG/arabinose and flow rate inputs can be encoded into frequency-modulated oscillations in the time domain where they can be independently extracted by Fourier transform. Thus, the measurement of a single clock history reveals the activities both underlying clock networks.

We began by characterizing the frequency response curves for both the intracellular and quorum clocks in isolation, finding ranges of 7–25 min and 55–95 min, respectively, when sweeping IPTG/arabinose and flow rate inputs (Fig. 3b, top: intracellular clock in araC+ strain and bottom: quorum clock, original study data[17]). We then measured trajectories taken from the coupled clock system and extracted the frequency components of both clocks by Fourier transform (Fig. 3c and Power spectra analysis). In sweeping IPTG/arabinose inducers, we found the frequency response of the intracellular clock contribution to the multispectral reporter to be unchanged by the inclusion of the quorum clock, where the intracellular frequency response to IPTG/arabinose was equivalent to the isolated clock (Fig. 3d, top: coupled and Fig. 3b, top: isolated). We then swept flow rates at 3 fixed inducer levels, finding distinct response curves for the quorum clock contribution to the multispectral reporter shifted in accordance with our model for ClpXP-mediated frequency modulation by the intracellular clock (Fig. 3d, bottom). Thus, to decode a given pair of

IPTG/arabinose and flow rate inputs, we first recover the intracellular clock frequency as a measure of IPTG/arabinose and then use the corresponding quorum clock response curve to measure flow rate.

To extend rapid coupling to greater spatial scales, we added a genetic H_2O_2 signaling[21] cassette to the network and observed synchronization at the multi-colony level (Fig. 4a and Supplementary Video 4). In conducting these experiments, we also observed H_2O_2-mediated interaction between the native stress response network and our synthetic circuit at ClpXP (Fig. 4b). In the original design, H_2O_2 synchronized quorum clock oscillations by transcriptional upregulation of the lux promoter via the aerobic response control system ArcAB[21]. In addition to transcriptional increase (Fig. 4c, top), we found an increase in the apparent degradation rate with H_2O_2 (Fig. 4c, bottom and Extended Data Fig. 4a–b), consistent with increased ClpXP activity in response to externally provided H_2O_2. The coupled increases in transcriptional output and effective ClpXP degradation rate in response to H_2O_2 also tightens the period distribution at the multi-colony level by mitigating the effects of period variation in an individual colony (Fig. 4c, top and Extended Data. Fig. 5c–d).

Engineering synthetic circuits composed of interacting modules is an ongoing effort[1–4] that has generally relied on transcription and translation, with less attention paid to post-translational coupling mechanisms[22]. Protease competition offers the advantages of rapid response, modularity with distinct recognition sequences, and simultaneous control over multiple circuits with protease adapters[23, 24]. More generally, in natural biological networks, competition for cellular resources (e.g., metabolites, enzymes, transcription factors, binding sites) produces nonlinear coupling effects that serve to reduce noise, increase sensitivity to input concentrations, and discriminate between multiple inputs[12, 25–28]. We envision that coordinating engineered circuits via built-in cellular processes—what we term “host-linked” coupling—has the potential to produce more sophisticated circuits by facilitating robust signaling between synthetic modules.

Methods

Strains and Plasmids

The oscillator plasmids were constructed by modifying and combining published constructs[17, 19, 21] by PCR reactions and all circuit components except *luxR* were tagged by PCR with a carboxy-terminal ssrA tag (AANDENYALAA)[11] for fast degradation. We placed the activator and reporting elements (LuxI/CFP and YFP) on one vector (IRAP2, Kan/ColE1) and the repressing elements (AiiA and LacI) on a second vector (IRAP3, Amp/p15A). The TS constructs were constructed by adding various TS repeat inserts between the CFP and the LAA tag. For example, for 2TS, the amino acid sequence “TSTS” was inserted immediately before the degradation tag “AAN-DENYALAA”. The AAV construct was constructed by replacing the “LAA” portion of the degradation tag with “AAV”.

Microfluidics and Microscopy

Image acquisition was performed on a Nikon TI and images were acquired using a Photometrics CoolSnap cooled CCD camera or Photometrics QuantEM EMCCD camera, both controlled by Nikon Elements software. The cells were imaged inside a microfluidic device with the ability to mix or switch between two different media sources. On the day of the experiment, 50 μL of an overnight culture was diluted in 50mL of LB (Difco) + antibiotics. When cells reached an OD_{600} of 0.1, cells were spun down and resuspended in 5mL of fresh media and loaded into the device. Three devices were used to study populations of varying sizes: small colony (100 cells)[29], large colony (5,000 cells)[17], and multiple large colonies (500 colonies of 5,000 cells[21].

Data Analysis

Single cell and individual trap fluorescent trajectories were obtained from time-lapse images using our previously developed algorithms [21, 29] and builtin MATLAB® functions. We identified peaks and troughs from these trajectories and used these values to calculate periods and amplitudes. To calculate the coupling delay in Figure 1A and offset time in 1C we measured the difference between the 10% amplitude points of trajectory pairs. The induction time was measured from induction start time to 10% amplitude of the induced module. To extract both frequencies from time series data, we performed Fourier transforms using the Lomb-Scargle algorithm. We used two sequential transforms to isolate each component separately. First, we used a band-pass filter (5 – 25 min) to extract the fast intracellular clock component. Then, we filtered out these fast frequencies using a second band-pass filter (75 – 150 min) to extract the slower quorum clock component. Finally, we overlay the 2 power spectra, preserving the relative amplitude of the peaks.

Extended Data

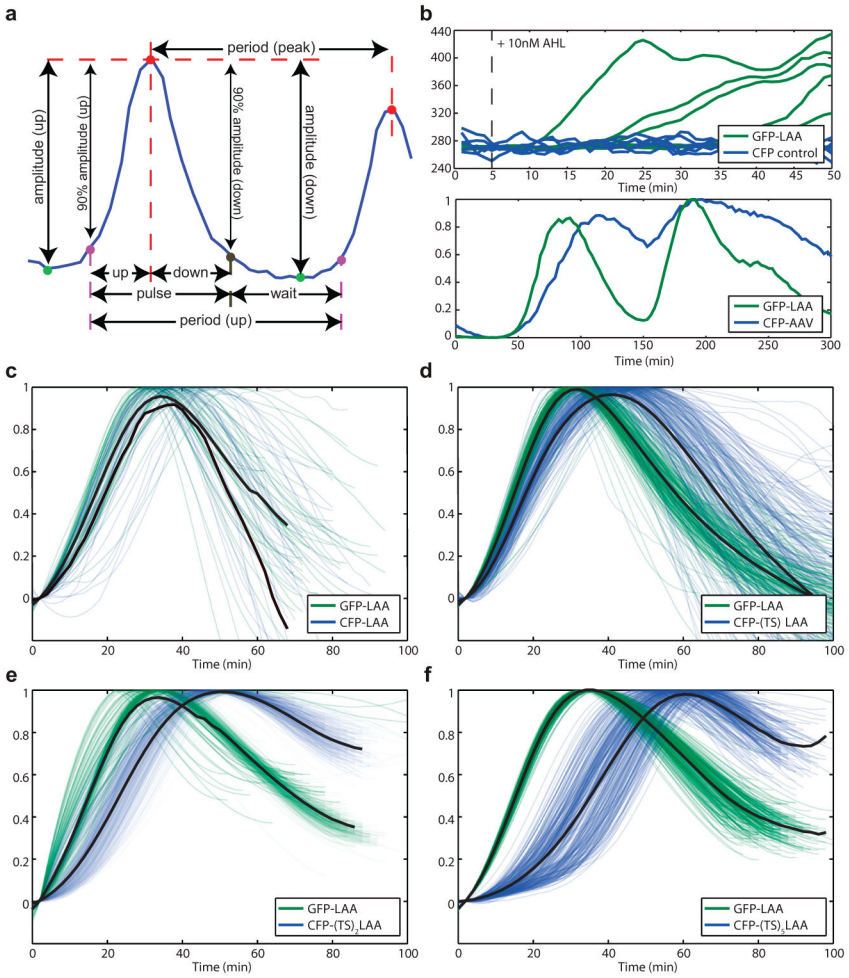

Extended Data Fig. 1.

Increasing length of the TS linker sequence results in increasing downstream module degradation delay. (a) Detailed breakdown of single fluorescent trajectory analysis. Peaks are identified in red, troughs in green, upslope 10% points in purple and downslope 10% points in dark beige. The two period measurements are peak to peak and the time between two successive 10% upslope points. (b) Top: sfGFP does not show bleed-over into CFP fluorescence channel. Induction of sfGFP with 10nM AHL (dashed line) showed increase in fluorescence of sfGFP, which was not detected in CFP channel. Bottom: the use of the published AAV degradation tag[30] shows delay in the downstream module degradation of 15min. (c) Without the TS linker sequence, there is very little delay in downstream module degradation. (d) Single TS linker sequence results in 10 min delay. (e) Double TS linker sequence results in 16 min delay, similar to that of AAV degradation sequence. (f) 5-TS linker sequence results in 25 min delay (data shown in panels c–f was used to generate Fig. 1C).

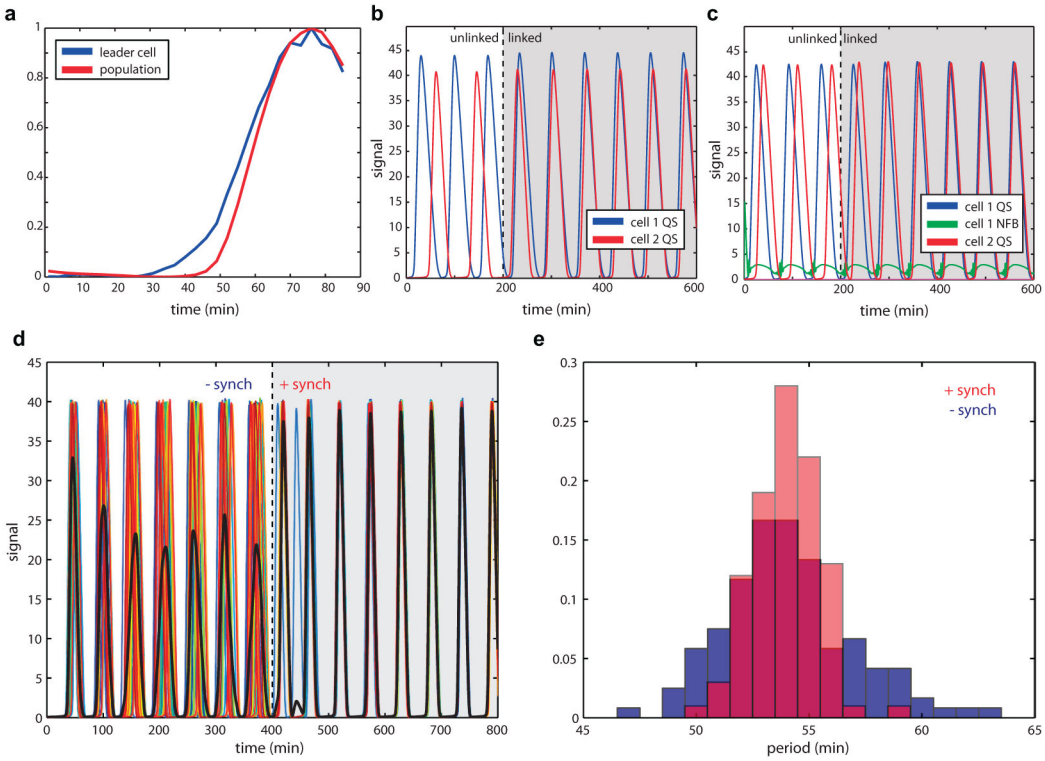

Extended Data Fig. 2.

Cell-cell communication by AHL reduces variability in the quorum clock. (a) Individual "leader" cells show early activation of quorum clock proteins relative to the mean population response. (b) In a 2-cell simulation, cells 1 and 2 start out unlinked with slightly different constitutive production of AiiA and LuxI (α_0). At t = 100min the two cells are linked through external AHL in the media, showing the cell with slower dynamics (2) linking up to cell 1 with shorter periods. (c) Cells 1 and 2 start out unlinked with cell 1 including intracellular clock dynamics (green) that result in higher frequency oscillations in cell 1. When the cells are linked (t =100), the slower cell 2, without the intracellular clock, links on to the faster cell through external AHL communication between the cells. (d) Trajectories of 20 cells with noisy constitutive production at lux promoter synchronize when their external AHL pool is mixed at t = 400min. Mean trajectory is shown in black. (e) Period variability after cell synching (red) is lower than in individual cells (blue).

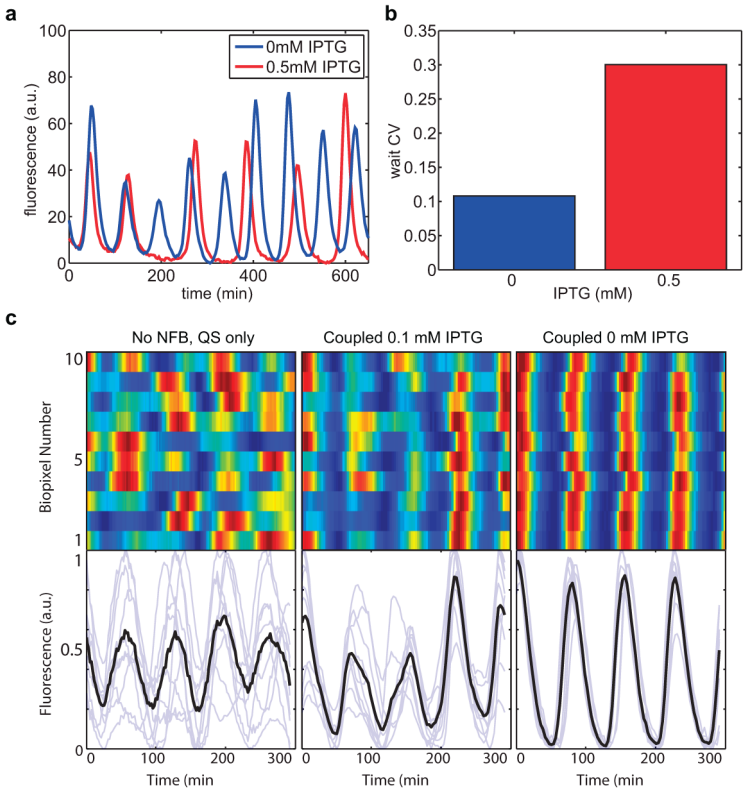

Extended Data Fig. 3.

The intracellular clock increases robustness in the coupled oscillator system by reducing the period of the quorum clock. (a) Removal of IPTG, which increases intracellular clock strength, leads to more regular oscillations (experimental). (b) The decrease in variability of the inter-pulse time of the coupled oscillator without IPTG suggests that the intracellular clock plays a significant role in the inter-pulse dynamics (experimental). (c) At very high flow rate, the quorum clock oscillates irregularly. Tuning up the intracellular clock reduces the quorum clock period, restoring regular oscillations and allowing for global level synchronization between colonies due to H_2O_2 biopixel couping. Genetic addition of the intracellular clock (0.1mM IPTG) helps synchronize the quorum clock at high flows (430μm=s). Increasing the strength of the intracellular clock with removal of IPTG further enhances H_2O_2 inter-colony synchronization (experimental).

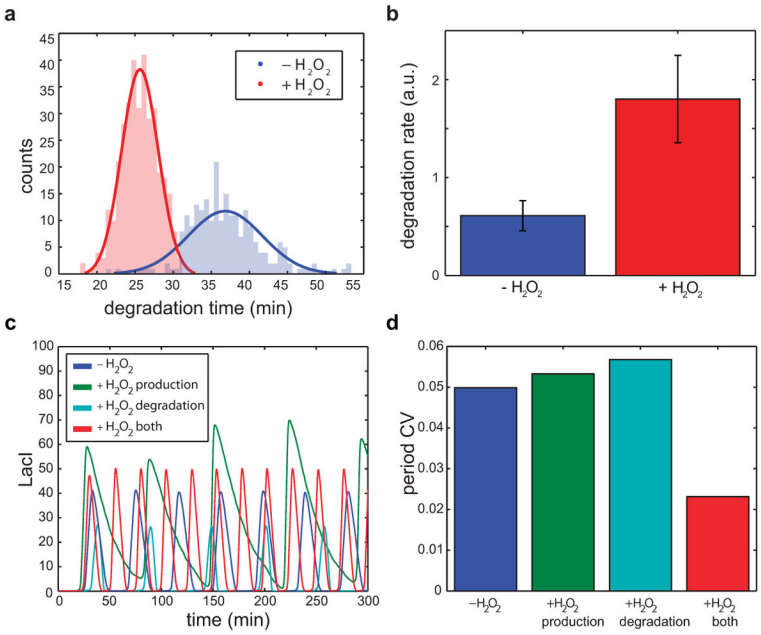

Extended Data Fig. 4.

H_2O_2 increases degradation rate by ClpXP that, in combination with transcriptional increase at the *lux* promoter, decreases variability in the oscillator period. (a) There is a significant decrease in the degradation time due to H_2O_2 (experimental). (b) This is due to effective increase in ClpXP degradation rate (experimental). (c) H_2O_2 activation of lux promoter alone would only increase the amplitude of quorum clock oscillations. Similarly, H_2O_2 -dependent increase in ClpXP activity results only in steeper degradation and longer inter-pulse duration. Combination of the two effects leads to increase in amplitude and decrease in inter-pulse duration, which matches experiments (model). (d) Individually the two H_2O_2 effects do little to lower the quorum clock period CV, which is reduced when both are present (model).

Supplementary Material

Refer to Web version on PubMed Central for supplementary material.

Acknowledgments

This work was supported by the National Science Foundation (MCB-1121748) and by the San Diego Center for Systems Biology (NIH Grant P50 GM085764) and the Department of Defense National Defense Science and Engineering Graduate Fellowship (AP). We would like to thank Tal Danino, Meng Jin, Chris Rivera, Omar Din, and John De Friel for critical reading of the manuscript. We would also like to thank two anonymous reviewers for critical comments that greatly strengthened the manuscript.

References

1. Moon TS, Lou C, Tamsir A, Stanton BC, Voigt CA. Genetic programs constructed from layered logic gates in single cells. Nature. 2012; 491:249–253. [PubMed: 23041931]
2. Siuti P, Yazbek J, Lu TK. Synthetic circuits integrating logic and memory in living cells. Nature biotechnology. 2013

3. Tigges M, Marquez-Lago T, Stelling J, Fussenegger M. A tunable synthetic mammalian oscillator. Nature. 2009; 457:309–312. [PubMed: 19148099]
4. Xie Z, Wroblewska L, Prochazka L, Weiss R, Benenson Y. Multi-input rnai-based logic circuit for identification of specific cancer cells. Science Signaling. 2011; 333:1307.
5. Lou C, Stanton B, Chen YJ, Munsky B, Voigt CA. Ribozyme-based insulator parts buffer synthetic circuits from genetic context. Nature biotechnology. 2012; 30:1137–1142.
6. Del Vecchio D, Ninfa AJ, Sontag ED. Modular cell biology: retroactivity and insulation. Molecular systems biology. 2008; 4
7. Nandagopal N, Elowitz MB. Synthetic biology: Integrated gene circuits. Science. 2011; 333:1244–1248. [PubMed: 21885772]
8. Fredriksson Å, et al. Decline in ribosomal fidelity contributes to the accumulation and stabilization of the master stress response regulator σs upon carbon starvation. Genes & development. 2007; 21:862–874. [PubMed: 17403784]
9. Merrikh H, Ferrazzoli AE, Bougdour A, Olivier-Mason A, Lovett ST. A dna damage response in escherichia coli involving the alternative sigma factor, rpos. Proceedings of the National Academy of Sciences. 2009; 106:611–616.
10. Cookson NA, et al. Queueing up for enzymatic processing: correlated signaling through coupled degradation. Molecular systems biology. 2011; 7
11. Keiler K, Waller P, Sauer R. Role of a peptide tagging system in degradation of proteins synthesized from damaged messenger rna. Science. 1996; 271:990. [PubMed: 8584937]
12. Goldbeter A, Koshland DE. An amplified sensitivity arising from covalent modification in biological systems. Proceedings of the National Academy of Sciences. 1981; 78:6840–6844.
13. Rosenfeld N, Alon U. Response delays and the structure of transcription networks. Journal of molecular biology. 2003; 329:645–654. [PubMed: 12787666]
14. Hooshangi S, Thiberge S, Weiss R. Ultrasensitivity and noise propagation in a synthetic transcriptional cascade. Proceedings of the National Academy of Sciences of the United States of America. 2005; 102:3581–3586. [PubMed: 15738412]
15. Mika F, Hengge R. A two-component phosphotransfer network involving arcb, arca, and rssb coordinates synthesis and proteolysis of σs (rpos) in e. coli. Genes & development. 2005; 19:2770–2781. [PubMed: 16291649]
16. Pruteanu M, Hengge-Aronis R. The cellular level of the recognition factor rssb is rate-limiting for σs proteolysis: implications for rssb regulation and signal transduction in σs turnover in escherichia coli. Molecular microbiology. 2002; 45:1701–1713. [PubMed: 12354235]
17. Danino T, Mondragón-Palomino O, Tsimring L, Hasty J. A synchronized quorum of genetic clocks. Nature. 2010; 463:326–330. [PubMed: 20090747]
18. Ferry M, Razinkov I, Hasty J. Microfluidics for synthetic biology from design to execution. Methods Enzymol. 2011; 497:295. [PubMed: 21601093]
19. Stricker J, et al. A fast, robust and tunable synthetic gene oscillator. Nature. 2008; 456:516–519. [PubMed: 18971928]
20. Prindle A, et al. Genetic circuits in salmonella typhimurium. ACS synthetic biology. 2012; 1:458–464. [PubMed: 23097749]
21. Prindle A, et al. A sensing array of radically coupled genetic/biopixels/'. Nature. 2011; 481:39–44. [PubMed: 22178928]
22. Grünberg R, Serrano L. Strategies for protein synthetic biology. Nucleic acids research. 2010; 38:2663–2675. [PubMed: 20385577]
23. McGinness KE, Baker TA, Sauer RT. Engineering controllable protein degradation. Molecular cell. 2006; 22:701–707. [PubMed: 16762842]
24. Griffith KL, Grossman AD. Inducible protein degradation in bacillus subtilis using heterologous peptide tags and adaptor proteins to target substrates to the protease clpxp. Molecular microbiology. 2008; 70:1012–1025. [PubMed: 18811726]
25. Burger A, Walczak AM, Wolynes PG. Abduction and asylum in the lives of transcription factors. Proceedings of the National Academy of Sciences. 2010; 107:4016–4021.

26. Mukherji S, et al. Microrna s can generate thresholds in target gene expression. Nature genetics. 2011; 43:854–859. [PubMed: 21857679]
27. Buchler NE, Louis M. Molecular titration and ultrasensitivity in regulatory networks. Journal of molecular biology. 2008; 384:1106–1119. [PubMed: 18938177]
28. Strogatz S. Nonlinear dynamics and chaos: with applications to physics, biology, chemistry and engineering. 2001
29. Mondragón-Palomino O, Danino T, Selimkhanov J, Tsimring L, Hasty J. Entrainment of a population of synthetic genetic oscillators. Science. 2011; 333:1315. [PubMed: 21885786]
30. Andersen JB, et al. New unstable variants of green fluorescent protein for studies of transient gene expression in bacteria. Applied and environmental microbiology. 1998; 64:2240–2246. [PubMed: 9603842]

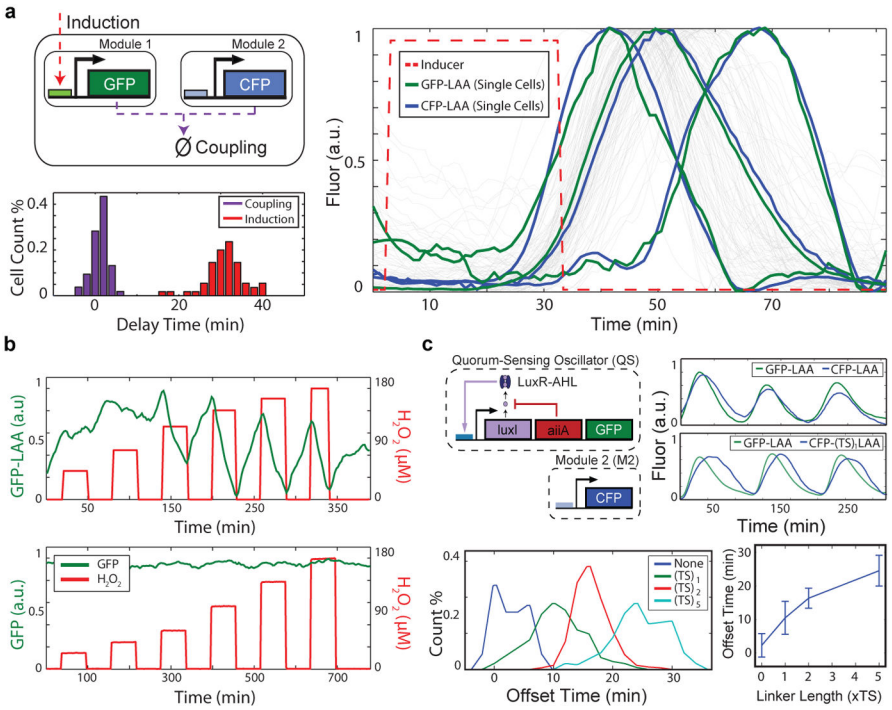

Fig. 1.

A rapid post-translational coupling platform based on shared degradation. (a) We measured the delays associated with module-module coordination by ClpXP (1±1 min) and input-output response via transcription/translation (31±5 min) in a single experiment by inducing the *lux* promoter and tracking the response of sfGFP-LAA (*lux* promoter) and CFP-LAA ($P_{lac/ara-1}$promoter) in single cells (55 cell trajectories). (b) Rapid (< 2 min, our experimental timestep) induction of protein degradation by externally provided H_2O_2 produces reversible changes in ClpXP load in response to obstruction of RssB[8, 9, 15]. (c) To use post-translational coupling to drive downstream modules, we linked a quorum clock to a constitutively expressed fluorescent protein via the addition of identical LAA tags. With identical degradation tags, the constitutive module couples tightly to the quorum pacemaker. The addition of a variable-length linker (TS repeats) before the degradation tag phase-shifts the degradation dynamics, where longer linkers produced longer delays. The error bars indicate s.d. of offset time, centered at the mean (50–200 cells for each TS-linker length).

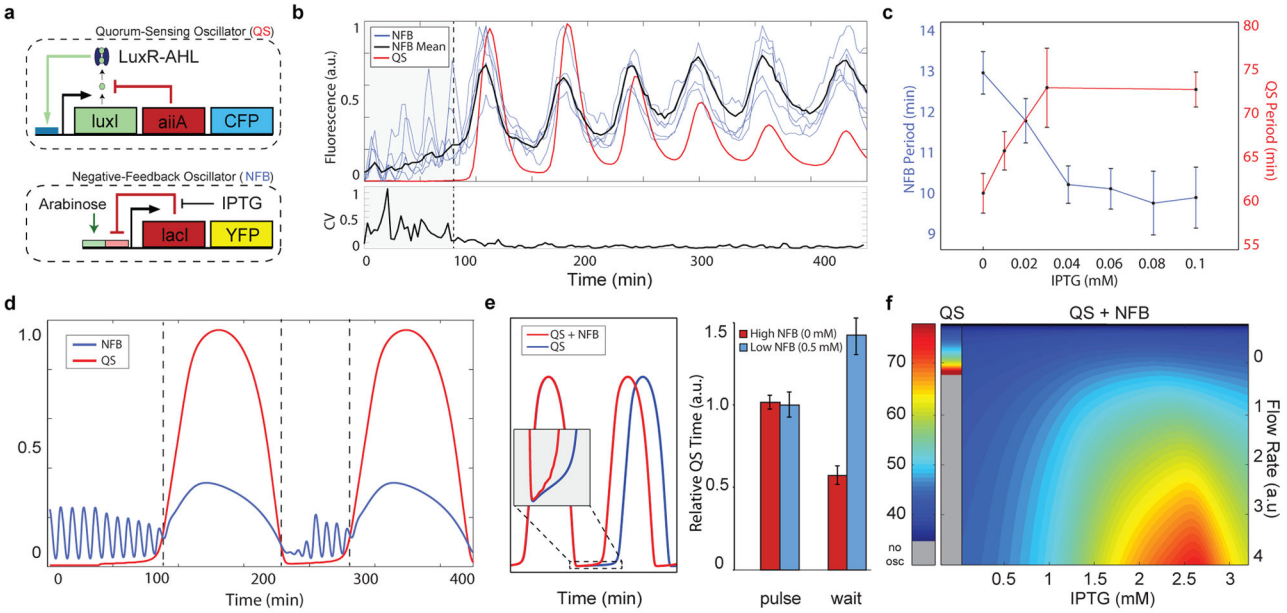

Fig. 2.

Post-translationally linked genetic clocks at multiple scales. (a) The network is composed of coupled intracellular[19] and quorum clocks[17]. The intracellular clock oscillates as a result of delayed negative feedback on its own promoter and its period is tunable by IPTG/arabinose. Quorum clock oscillations are tunable by media flow rate and are synchronized via AHL at the colony level. (b) The coupled intracellular-quorum clock system oscillates asynchronously in small populations and transitions to synchronized oscillations in larger populations once the quorum clock fires. Despite lacking a mode of cell-cell communication itself, the coefficient of variation of the intracellular clock drops markedly via host-linked coupling with the quorum clock (bottom, data from 28 single cell traces). (c) IPTG reduces the intracellular clock period in small cell populations without the quorum clock (blue) and increases the coupled period in larger populations with the quorum clock (red). Each data point taken from 10–30 oscillatory peaks. The error bars indicate s.e.m. of the period, centered at the mean. (d) In our computational model, load-mediated coupling allows the intracellular clock to modulate the quorum clock period via degradation coupling at ClpXP, where the intracellular clock continues oscillating between coupled pulses and accelerates the pulse onset. (e) This adaptive form of pulse frequency modulation ensures that the pulse dynamics remain unchanged while the inter-pulse duration is adjusted (left: model and right: experimental, 6–9 oscillatory peaks) The error bars indicate s.e.m. of relative quorum clock period. (f) This mechanism also makes the coupled system more robust by enabling oscillation at higher media flow rates.

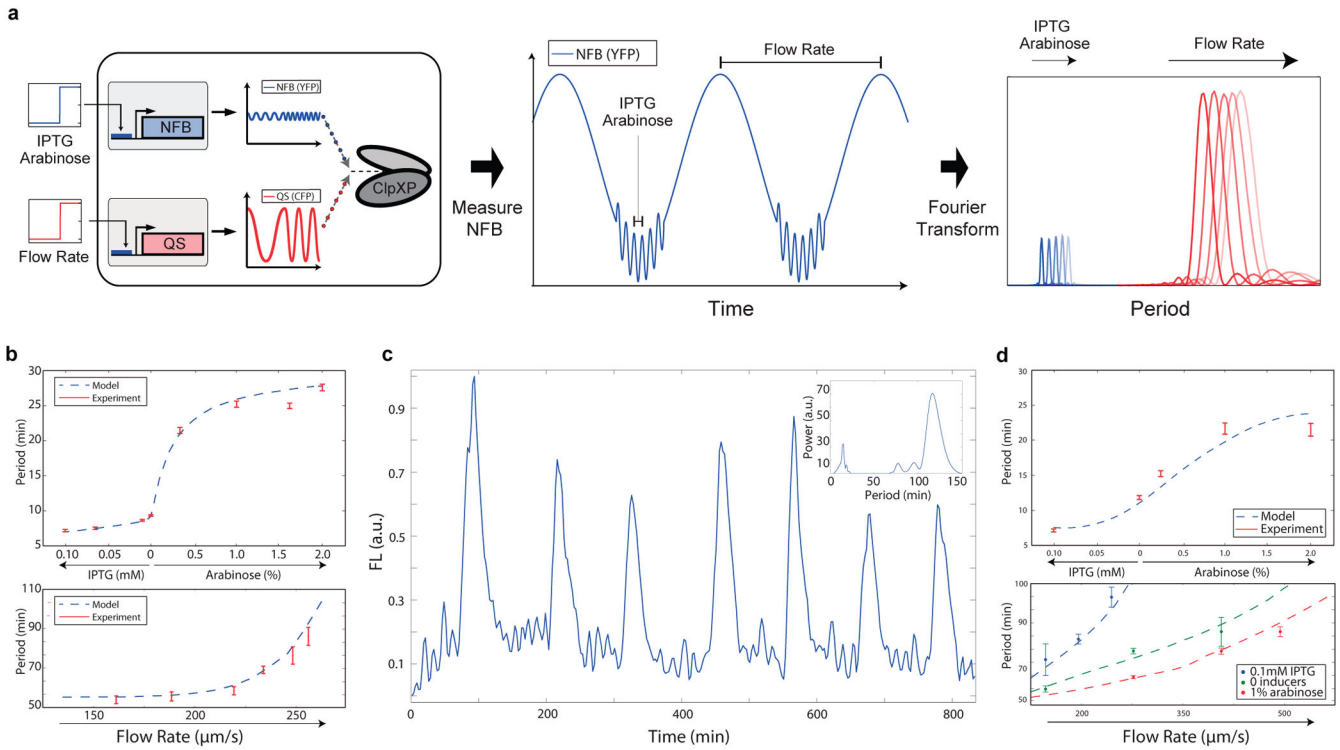

Fig. 3.

Genetic multispectral encoding. (a) Separate IPTG/arabinose and flow rate inputs are encoded into frequency-modulation oscillations that can be measured from the time series of the reporter for the intracellular clock. This engineered system is capable of encoding information from two underlying networks into a single multispectral time series. (b) Frequency response curves generated from experimental data and computational models for the intracellular clock (top, data from 30 single cell traces each) and quorum clock (bottom, model applied to data from the original study[17]) in isolation. The error bars indicate s.e.m. of the period, centered at the mean. (c) In the coupled system, frequency-modulated oscillations from both clocks can be observed in the output of the intracellular clock and extracted by inverse Fourier transform (inset, methods in Extended Data Data Analysis). (d) Independent recovery of both IPTG/arabinose and flow rate inputs, where the frequency response of the intracellular clock to IPTG/arabinose is equivalent to the isolated clock (top) and the frequency response of the quorum clock is shifted by the intracellular clock (bottom). Periods calculated from 5–10 single cell traces for each condition. The error bars indicate s.e.m. of the period, centered at the mean.

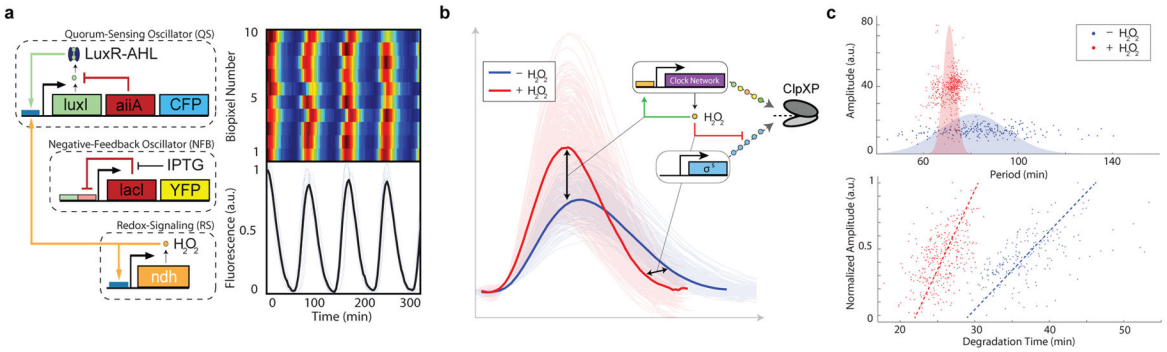

Fig. 4.

Post-translational coupling at the multi-colony level. (a) At the multi-colony level, interaction of H_2O_2 generated by redox signaling with the cellular stress response network synchronizes quorum clock oscillations between colonies. Traces taken from 10 separate colonies across the array. (b) Host-linked oscillations change distinct aspects of the waveform in response to H_2O_2 produced by the enzymatic activity of NDH. With H_2O_2, oscillations have larger amplitudes and steeper downslopes, revealing increases in both transcription and degradation produced by the interaction of the synthetic clock network with the native stress response. (c) H_2O_2 increases the oscillatory amplitude while decreasing the required degradation time, revealing an increase in ClpXP activity. This increase in ClpXP capacity in response to H_2O_2 serves to mitigate the effects of transcriptional noise by minimizing the effects of amplitude variation on the period, resulting in a tightening of the period distribution with H_2O_2 (model: Extended Data Fig. 4c–d).